6. ANTARCTICA

a. Overview—R. L. Fogt

The calendar year 2009 was relatively calm, climatologically speaking, for much of Antarctica, especially compared to the past two years which included ice shelf collapses juxtaposed with record-high sea ice extent. However, the total ice sheet melt during austral summer 2008/09 was the lowest of the 30-yr satellite record with no melt detected on the Ronne-Filchner and Ross Ice shelves, among other regions. In 2009, the polar atmosphere temperatures were persistently above average in the mid- to-lower troposphere during the winter. The latter half of the year was marked with short-lived anomalies lasting about one month. Nonetheless, the tropical El Niño event in late 2009 did influence Antarctica, particularly through ridging in the South Pacific. In turn, this created anomalous meridional temperature advection patterns that subsequently led to regional sea ice extent and concentration anomalies and decreased precipitation to the west of the Antarctic Peninsula.

With the close of 2009 also comes the end of the first decade of the 21st Century. Although Antarctic climate records are much shorter than the rest of the globe, there were still many interesting and noteworthy occurrences during this last decade. A few of these are highlighted in Fig. 6.1, which shows annual and seasonal averages of the decadal mean temperature anomalies at Faraday/Vernadsky and Marambio, situated on the Western and Eastern Antarctic Peninsula, respectively, and the decadal mean Southern Hemisphere Annular Mode (SAM) index anomalies. Notable Antarctic climate events of the last decade include:

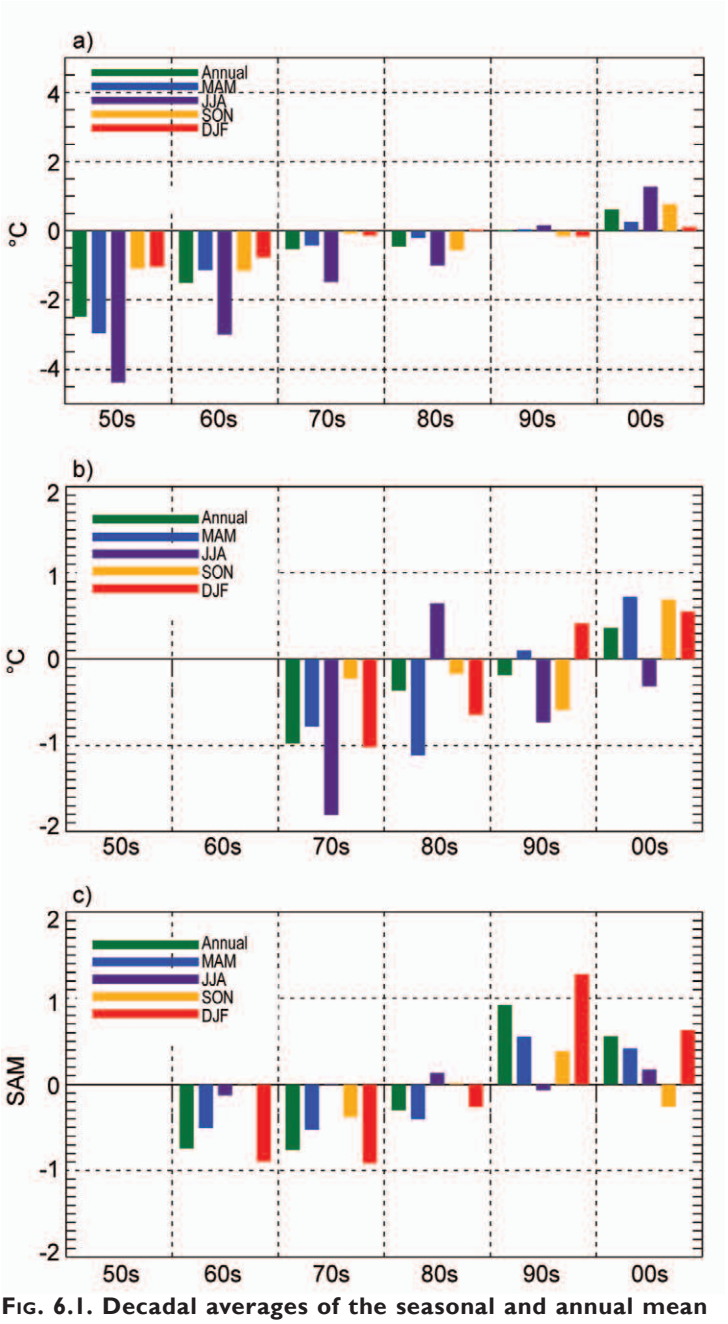

Fig. 6.1. Decadal averages of the seasonal and annual mean anomalies for (a) temperature at Faraday/Vernadsky, (b) temperature at Marambio, and (c) SAM index (http://www.antarctica.ac.uk/met/gjma/sam.html). See Fig. 6.4a for locations of stations used in 6.1a–b.

- Observations indicate continued rapid warming of the Antarctic Peninsula. The warming on the western Peninsula is most marked during austral winter (June–August; Fig. 6.1a) while the warming on the eastern Peninsula is most marked during austral summer (December–February; Fig. 6.1b). The Peninsula warming trends are approximately five times larger than the global mean warming and are likely associated with anthropogenic greenhouse gas increases (Gillett et al. 2008).
- Based on a statistical temperature reconstruction, West Antarctica has been warming at a rate of 0.1°C decade^{-1} over the last 50 years (Steig et al. 2009).
- Based on surface observations, interior and coastal East Antarctica have remained stable during the last decade, with no significant warming or cooling trend (Turner et al. 2005).

- Significant ice loss has occurred along the Antarctic Peninsula and West Antarctica in the last decade. In 2002, the Larsen B Ice Shelf on the east side of the Peninsula disintegrated, likely due to the regional warming (see above) (Marshall et al. 2006). In 2008/09, part of the Wilkins Ice Shelf on the west side of the Peninsula collapsed, more likely due to influences other than regional warming (Scambos et al. 2009). More recently, ice loss has been reported in the Pine Island Bay region of West Antarctica (Rignot 2002), due perhaps to oceanic influences (Payne et al. 2007).
- All-time positive records of continent-averaged sea ice extent were reached in December 2007, and March–April 2008, in conjunction with a small but significant increase in overall sea ice extent over the last 30 years (Fogt et al. 2009a). Embedded in this signal are large regional departures: during the last three decades there was an anomalous decrease in sea ice in the Amundsen/Bellingshausen Seas, especially in winter, and an anomalous increase in sea ice extent in the Ross Sea sector.
- The 2008/09 Antarctic-wide austral summer snowmelt was the lowest in the 30-yr history (Tedesco and Monaghan 2009).
- Many of the climate impacts can be related back to changes in the overlying atmospheric circulation and, in particular, the average positive phase of the SAM. Figure 6.1c shows that although the SAM weakened somewhat during the 2000/09 decade, it still remained positive on average (compared to the 1979–2008 mean) during all seasons except austral spring. It is widely accepted that the strong positive phase of the SAM in austral summer can be traced back to stratospheric ozone depletion and greenhouse gas increases (Fogt et al. 2009b; Arblaster and Meehl 2006; Shindell and Schmidt 2004; Thompson and Solomon 2002).
- The Antarctic ozone hole reached its maximum area (27.7 million km^2) on 24 September 2006, larger than the North American continent. Due to large interannual variability, it is unclear yet whether or not the ozone hole has begun a slow recovery process.

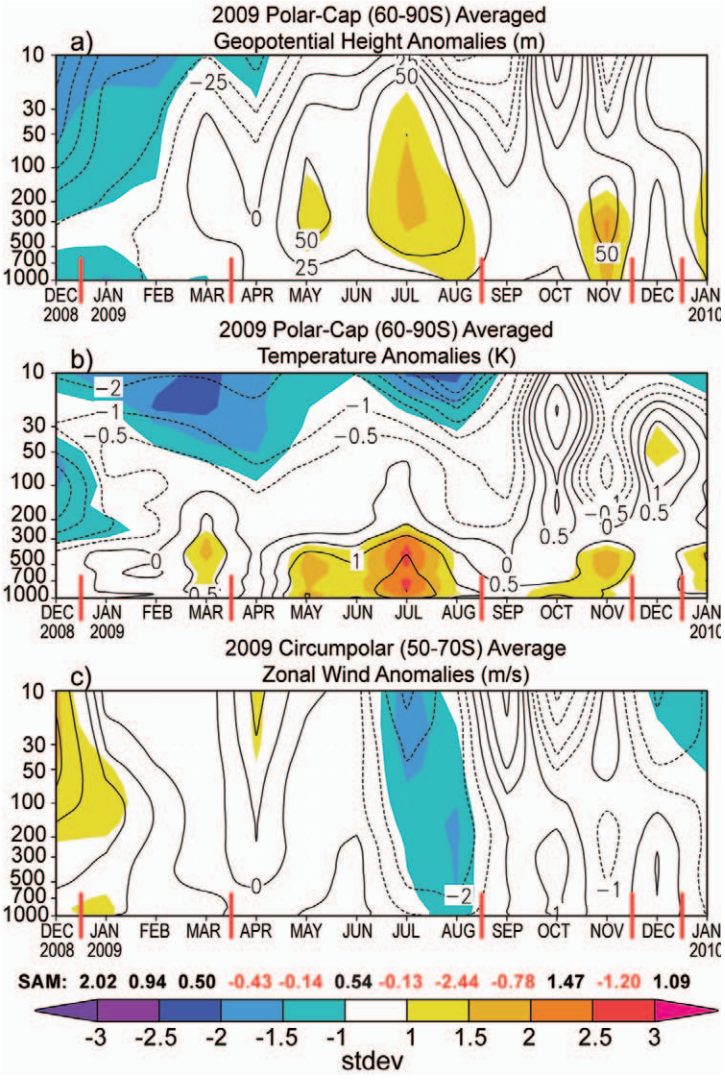

Fig. 6.2. Zonally-averaged climate parameter anomalies for the southern polar region in 2009 relative to the 1979–2008 period: (a) polar cap averaged geopotential height anomalies (m); (b) averaged temperature anomalies (K); (c) averaged wind anomalies (m s^{-1}). Absolute anomaly values are contoured, and the panels are shaded according to how many standard deviations the anomalies are from the 1979–2008 mean (color bar at bottom for scale). Red vertical bars indicate the four separate periods shown as spatial climate anomalies for 2009 in Fig. 6.3. Primary contour interval is 50 m in (a), 1 K in (b), and 2 m s^{-1} in (c), with additional contours at ± 25 m, ± 0.5 K, ± 1 m s^{-1} in (a), (b), and (c), respectively. Values for the SAM index are shown along the bottom in black and red. (Source: NCEP–NCAR reanalysis.)

Many of these impressive conditions during the last decade, and projections for the Antarctic climate over the next 100 years, are described in more detail in the Scientific Committee on Antarctic Research

(SCAR) report "Antarctic Climate Change and the Environment," which was released in November 2009. This report not only parallels the climate discussion on the following pages, but also includes paleoclimatic changes, oceanic changes, and changes in the marine/terrestrial biosphere.

b. Atmospheric circulation—R. L. Fogt and S. Barreira

Antarctic large-scale circulation anomalies during 2009 based on the NCEP–NCAR reanalysis are examined throughout the troposphere–stratosphere (Fig. 6.2) and at the surface (Fig. 6.3). Because the high southern latitude reanalysis data quality improves drastically at the start of the modern satellite era (Bromwich and Fogt 2004; Bromwich et al. 2007), reanalysis data is used starting in 1979. Dividing the circulation anomalies into groups was particularly challenging for 2009, as many of the anomalies were weak and only lasted for a short time, especially during the latter half of the year. Nonetheless, both Figs. 6.2 and 6.3 indicate that the beginning of the year was dominated by below-average heights/pressures from the surface up to 10 hPa, accompanied by weakly positive circumpolar zonal wind anomalies and positive tropospheric temperature anomalies. The positive surface temperature anomalies were most marked in East Antarctica (Fig. 6.3b), and there was a notable negative surface pressure anomaly in the South Pacific Ocean during January–March (> 2 standard deviations below the 1979–2008 mean). The clockwise circulation about this low pressure anomaly increased warm-air advection to the Peninsula, making the temperatures higher there during the early part of the year (Fig. 6.3b). Furthermore, both the northeastern Weddell and Bellingshausen Seas were free of sea ice during January and February, which is consistent with the circulation and temperature anomalies presented in Figs. 6.3a,b.

From April to August, comprising most of the polar winter, the above-average temperatures are seen throughout the Antarctic troposphere with positive pressure/height anomalies over the continent. This pattern was most marked in July, when temperature anomalies were > 2°C (from the surface up to 500 hPa; Figs. 6.2b and 6.3d) and more than two standard deviations above the 1979–2008 mean. Further, the positive height anomalies during this time period are matched with anomalously weak circumpolar zonal winds. Note, however, that the (SAM) index reached its lowest value for 2009 (-2.44) one month later, in August. Here the SAM magnitude is defined using the Marshall (2003) index, which is based on mean

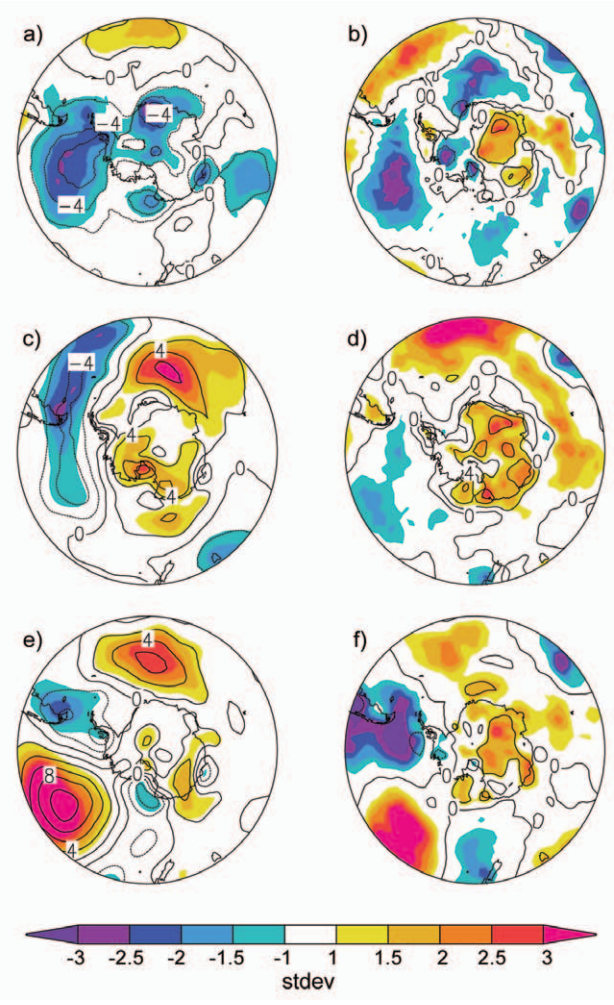

Fig. 6.3. (left) Surface pressure anomalies and (right) surface temperature anomaly contours relative to 1979–2008 climatology for (a,b) January–March 2009, (c,d) April–August 2009, and (e,f) September–December 2009. The shaded regions correspond to the number of standard deviations the anomalies are from the 1979–2008 mean, as in Fig. 6.2. (Source: NCEP–NCAR reanalysis.)

sea level pressure anomalies. Although the overall circulation anomalies were most marked in July, there was a one-month delay in timing of peak magnitude at the surface, clearly seen in the downward anomaly propagation from July–August in both geopotential height and circumpolar zonal winds (Fig. 6.2).

The above average near-surface temperatures continued through austral spring (September–November, Fig. 6.2b). During the end of the year the SAM index was relatively weak and nonstationary, altering between negative and positive states. Examining the spatial surface pressure anomalies (Fig. 6.3e) reveals that the circulation pattern during the end of the year shows a distinct wave train from the Pacific to Atlantic sectors, resembling the Pacific

South American Pattern (Karoly 1989). Further, the spatial temperature anomalies from 180°W–0° in Fig. 6.3f are readily explained by the ensuing meridional temperature advection changes resulting from the anomalous circulation. Of these, most notable was the strong positive pressure anomaly (>2.5 standard deviations) in the South Pacific, characteristic during El Niño events (Turner 2004). This circulation anomaly made the temperatures in the South America–Antarctic Peninsula region below average (> 2.5 standard deviations) and the central South Pacific above average (> 2.5 standard deviations) during the latter half of the year.

c. Surface manned and automatic weather station observations—S. Colwell, L. M. Keller, and M. A. Lazzara

The circulation anomalies are further examined and confirmed here using direct measurements of temperature, wind, and pressure at several manned and automatic weather stations across Antarctica. Fig. 6.4a displays the location of these stations. Two representative manned stations are displayed in Figs. 6.4b,c, and two automatic stations are displayed in Figs. 6.4d,e. A Google Earth file displaying the time series for each station described in this section can be found at: http://www.antarctica.ac.uk/met/momu/BAMS/anomalies.kml. The base period for calculating the anomalies was 1979–2008 for the manned stations and 1980–2008 for the automatic weather stations.

The temperatures in the northern part of the Antarctic Peninsula were below average for most of the year, with June, July, and August being especially cold at Bellingshausen and Marambio (Fig. 6.4c), although not breaking records. Further south on the Peninsula at Rothera station, the temperatures were slightly higher than average for most of the year. In the Weddell Sea region, the temperatures at Halley and Neumayer remained fairly close to the long-term average for most of the year, except for August, which was 3.5°C colder than average and October which was 4°C warmer than average. The pressures in August were much higher than average at Marambio (Fig. 6.4c; +14.8 hPa), Bellingshausen (+11.4 hPa), Rothera (+12.4 hPa) and Halley (+9.9 hPa), due to high pressure anomalies over the Weddell Sea (i.e., Fig. 6.3c).

Around the coast of East Antarctica the temperatures at Mawson, Davis, and Casey were generally higher than the long-term averages, although these stations experienced below-average temperatures at

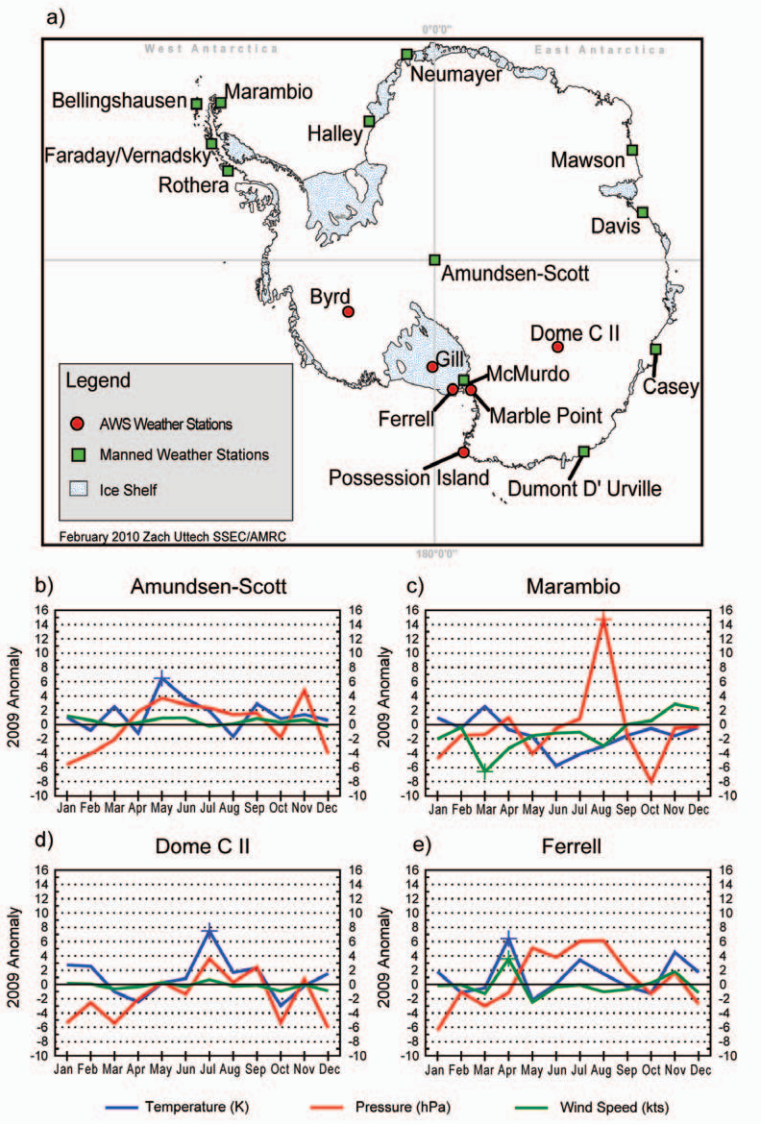

Fig. 6.4. (a) Locations of automatic and manned Antarctic weather stations described in Chapter 6. (b)–(e) 2009 Antarctic climate anomalies at four representative stations (two manned, and two automated). Monthly mean anomalies for temperature (K), MSLP (hPa), and wind speed (m s^{-1}) are shown, with plus signs (+) denoting all-time record anomalies for a given month at each station. Climatological station data starts in 1957 for Amundsen-Scott, 1970 for Marambio (1983 for Marambio wind speeds), and 1980/81 for the AWS records. The base period for calculating the anomalies was 1979–2008 (1980–2008 for the AWS records).

these stations in April, August, and December. At the South Pole Amundsen Scott station (Fig. 6.4b) they recorded its warmest ever May temperature of -51.4°C, which was 2.0°C higher than the previous warmest value in 1981. They also recorded their highest annual mean temperature of -47.9°C, which was 0.1°C warmer than the previous warmest year of 2002.

Records from automatic weather stations on the Ross Ice Shelf, West Antarctica, and the Polar Plateau were also analyzed. On the Ross Ice Shelf both Gill and Ferrell (Fig. 6.4e) reported record-high mean temperatures and record mean high wind speeds for April 2009, where Gill was around 10.0°C higher than the long-term April mean and Ferrell was 6.4°C higher. Marble Point, near the Ross Sea and McMurdo Station, reported a record high mean wind speed for April. In West Antarctica, Byrd station reported above-average temperatures in July, August, November, and December, as well as higher-than-normal pressure for April, July, August, and November, but no records were set. On the Polar Plateau, Dome C II (Fig. 6.4d) had a record high monthly mean temperature in July (7.5°C above the long-term mean). Possession Island, near Cape Adare at the northwest corner of the Ross Sea, also had a record high mean temperature for July (-17.0°C), and record high mean pressures for May and August (8.3 and 6.3 hPa respectively higher than normal), as reflected in Figs. 6.3c,d.

d. Surface mass balance—D. H. Bromwich and S.-H. Wang

Earlier studies (e.g., Bromwich et al. 2004; van den Broeke et al. 2006) suggest that precipitation-minus-evaporation/sublimation (P-E) closely approximates the surface mass balance over most of Antarctica, with precipitation being the dominant term at regional and larger scales. Precipitation and evaporation fields from the Japanese Reanalysis (JRA; Onogi et al. 2007) were examined to assess Antarctic snow accumulation behavior for 2009. The evaporation in JRA was calculated from the surface latent heat flux variable. In comparison to other long-term global reanalyses (e.g., NCEP1 and NCEP2), JRA has higher model resolution, both horizontally and vertically, greater observational usage, and a more advanced model configuration (Onogi et al. 2007).

Figure 6.5 shows the JRA annual anomalies of P-E and mean sea level pressure (MSLP) for 2008 (Figs. 6.5b,d) and 2009 (Figs. 6.5a,c) to demonstrate the similarities and major differences between these years. In general, the annual anomalies over the high interior of the continent are small (within ± 50 mm yr^{-1}) in both years, consistent with the low amount of snow accumulation in this region. Most coastal regions in 2009 display much bigger P-E anomalies than during the previous year. The most negative P-E anomalies in 2009 can be observed to the west of the Antarctic Peninsula, in contrast to large positive anomalies over the Peninsula in 2008. In both years, the annual P-E anomalies are consistent with the mean atmospheric circulation implied by the MSLP anomalies (Figs. 6.5c,d). In 2008, a strong negative MSLP anomaly was observed in the Amundsen/Bellingshausen Seas (105°W, along with secondary negative MSLP

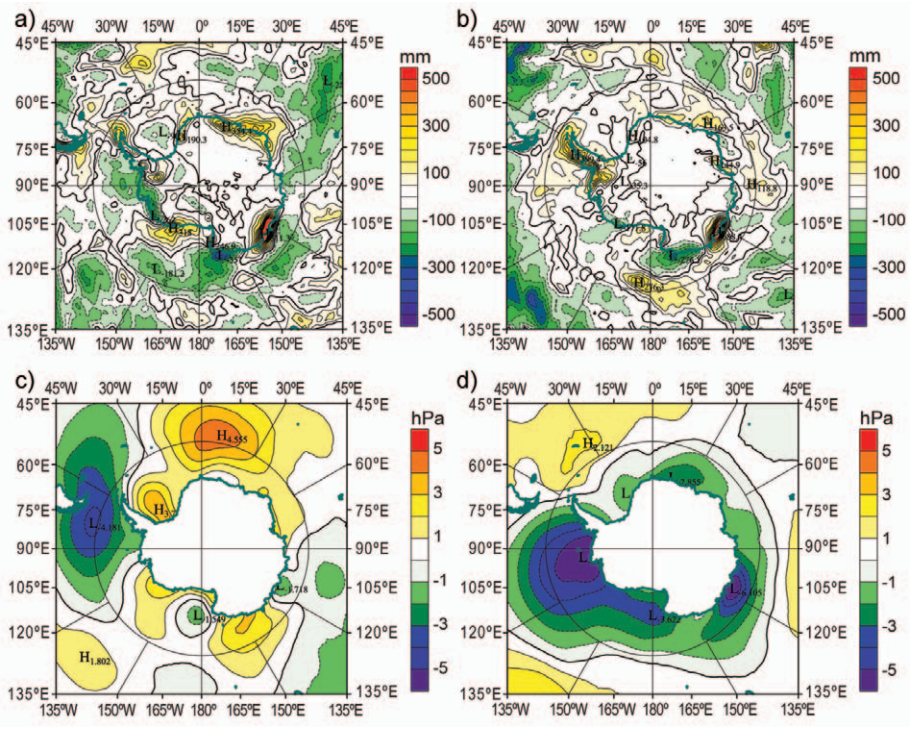

Fig. 6.5. Japanese Reanalysis annual precipitation minus evaporation (P-E) and annual mean sea level pressure anomalies: (a) 2009 P-E anomalies, departure from the 1979–2008 mean; (b) 2008 P-E anomalies, departure from the 1979–2007 mean; (c) 2009 annual mean sea level pressure anomalies; and (d) 2008 annual mean sea level pressure anomalies.

anomalies observed in the Ross Sea and along the Antarctic coast between 100°E to 140°E [Fig. 6.5d]). These circulation anomalies produced three P-E anomaly features along the Antarctic coast in 2008 (Fig. 6.5b): positive anomalies over the Ross Ice Shelf and near Casey station (110°E) and a negative center over the Balleny Islands (165°E). In 2009, a strong negative pressure anomaly center was observed near the Drake Passage (Fig. 6.5c). The circulation about this low pressure in 2009 produced stronger offshore flow and less precipitation to the west of the Antarctic Peninsula, leading to the P-E minimum along coastal West Antarctica (Fig. 6.5a). Further, 2009 was also marked with a positive MSLP anomaly center at 15°E (Fig. 6.5c). This pressure anomaly brought more moisture from the ocean into the region along the coast between 0° to 60°E, where the 2009 annual positive P-E anomalies have increased to more than double the 2008 values.

The austral spring (SON) and autumn (MAM) P-E anomalies (not shown) have the largest impact on 2009 annual P-E anomalies. The SON anomalies contribute nearly 40% of the annual P-E coastal values. A strong negative MSLP anomaly in SON 2008 from 120°E eastward to a dominant center near 100°W has been replaced by a strong positive center at 125°W, nearly a 20-hPa change (i.e., Fig. 6.3e). This indicates less-than-normal storm activity during the 2009 SON season that results in the change to the west of the Antarctic Peninsula from large positive to large negative P-E anomalies.

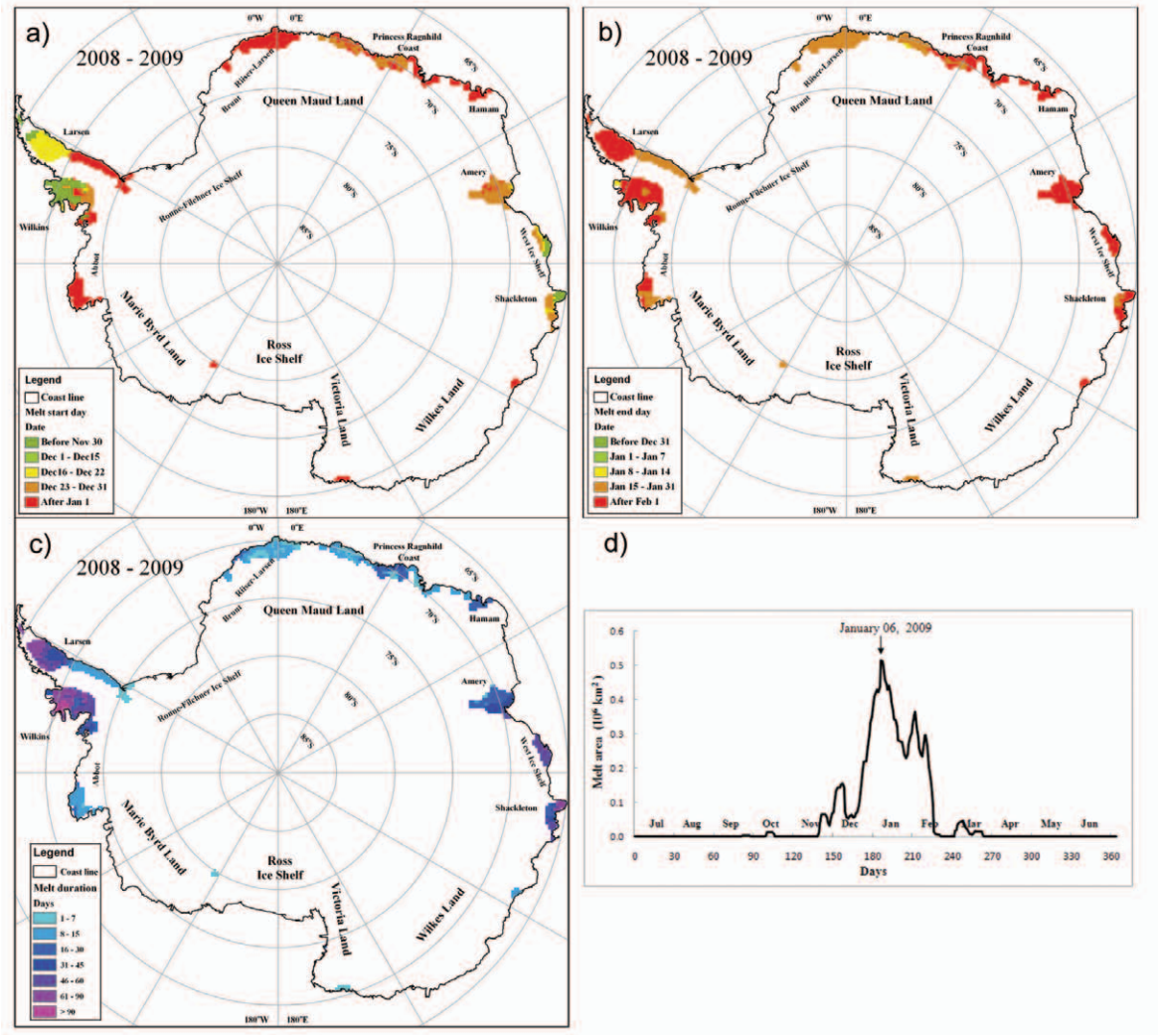

Fig. 6.6. Surface snow melt (a) onset date, (b) end date, (c) duration, and (d) melt area for the austral summer 2008/09 melt season.

e. 2008–2009 Seasonal melt extent and duration—L. Wang, K. C. Jezek, and H. Liu

Summer surface snow melt on the Antarctic Ice Sheet during 2008/09 was estimated using 19-GHz horizontal-polarization channel SSM/I data. We applied a wavelet transform-based edge detection method (Liu et al. 2005) to the daily time series of brightness temperatures for individual SSM/I grid cells to detect and track the surface melt occurrences. Surface melt extent and duration maps are shown in Fig. 6.6. The total melt extent is 681 900 km^2, which includes all areas with at least one day of surface melting during the 2008/09 austral summer. The melt extent covers only 4.9% of the continent, which is considerably smaller than the average melt percentage (about 9.3%) over the past 27 years (Liu et al. 2006). The integrated melt index (the summation over the continent of the product of melt duration times the pixel area) during 2008/09 is 20 533 000 day km^2. Both melt extent and melt index for the entire ice sheet are smaller than the last year (800 000 km^2 for melt extent and 24 354 000 day km^2 for melt index), consistent with the decreasing trend of the past six years. Melt extent and melt index for the austral summer 2008/09 are record lows for the period of passive microwave satellite observations that began in 1978 (Tedesco and Monaghan 2009).

The Antarctic Peninsula, Amery Ice Shelf, West Ice Shelf, and Shackleton Ice Shelf (see Fig. 6.6a for locations) have relatively longer melt durations than other regions. Abbot Ice Shelf and the small ice shelves in Queen Maud Land have melt durations of less than two weeks. No surface melt was detected on the Ronne-Filchner Ice Shelf, Ross Ice Shelf, Victoria Land, or on Wilkes Land (Fig. 6.6). The surface melt onset date and end date varies spatially, as shown in Figs. 6.6b,c. Surface melt events primarily took place in January (Fig. 6.6d).

f. Sea ice extent and concentration—R. A. Massom, P. Reid, S. Stammerjohn, and S. Barreira

After a maximum in zonally-averaged sea ice extent (based on the satellite passive microwave record) in December 2008 (monthly average of 11.2 x 10^6 km^2, or ~1.0 x 10^6 km^2 above the long-term mean for 1979–2008), anomalies in January 2009 were generally well above average (~0.8 x 106 km^2) but dipped dramatically to be slightly below average in February. For much of the rest of the year, overall sea ice extent and area were above average or close to average, with seasonal peaks in April (extent +1.0 x 10^6 km^2) and late September (+0.5 x 10^6 km^2). Starting in October, however, there was a decrease in zonally-averaged extent that lasted through mid-December 2009.

Embedded in the zonally-averaged sea ice extent are again strong regional contrasts in the sea ice record, in accordance with recent observations (e.g., Comiso and Nishio 2008; Stammerjohn et al. 2008). In many regions, and especially during early 2009, regional sea ice extent anomalies were generally consistent with long-term (30-year) regional trends (Fig. 6.7a): negative in the Bellingshausen Sea and western Weddell Sea (January through June/July), the W Pacific sector from ~90°E–120°E (February–December) and in the eastern Ross Sea (January–March); positive in the central-eastern Weddell Sea (January–June/July) and the western and central Ross Sea (January–June and January–October, respectively); and a largely neutral/mixed signal over much of the Indian Ocean sector (January–April), the W Pacific sector from 120°E–145°E (throughout the year), and the Amundsen Sea (January–May).

Not all regional sea ice extent anomalies were consistent with long-term (30-year) regional trends. Most notable was the regional departure from long-term trends that began in October 2009 that was associated with a distinct hemispheric wave-3 pattern in that month. Distinct sea ice extent anomalies occurred in two regions due to the presence of a high pressure anomaly centered on 120°W (reflected in Fig. 6.3e): positive in the Bellingshausen-Amundsen Seas (BAS) region and negative in the eastern Ross Sea (Fig. 6.7c). Similarly, a negative sea ice extent anomaly developed in the western Ross Sea, caused by a low MSLP/storm center west of the high pressure center (Fig. 6.3e). This coincides with the development (from October onwards) of a warm pool of SSTs in the central South Pacific that persisted through December. From October, departures in regional sea ice extent are up to 3.4 standard deviations away from the (untrended) mean and are in distinct contrast to the long-term regional trends. This is particularly evident by comparing the areas of the BAS-NW Weddell Sea and Ross Sea sectors for April (similar to the trend, Fig. 6.7e) and November (opposite to the trends, Figs. 6.7b,c).Other less obvious departures from the long-term mean were the large negative and positive anomalies that persisted in the NW and central-NE Weddell Sea (CNEWS) from January through July that subsequently advected eastwards with the surface waters of the Weddell Gyre (Venegas and Drinkwater 2001; Fig. 6.7a). This resulted in a switch to a strong negative anomaly in CNEWS accompanied by a strong positive anomaly from ~0°–60°E (inconsistent with

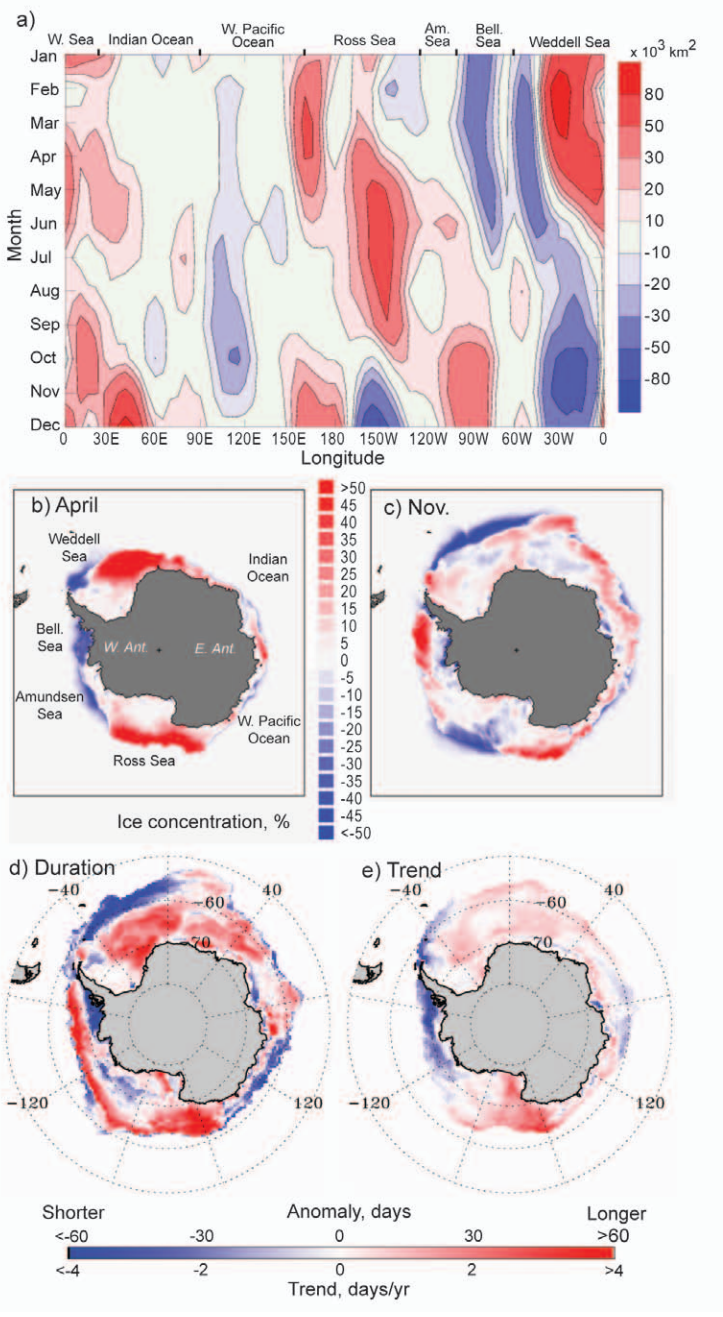

Fig. 6.7. (a) Hovmöller diagram of daily satellite-derived sea ice extent anomalies for 2009 (2009 minus the 1979–2008 long-term mean, in 10^3 km^2); (b) and (c) sea ice concentration anomaly maps for April and November 2009, respectively, derived versus the monthly means for 1979–2000 (total anomalies of 1.0 and 0.1 2 x 10^6 km^2, respectively) (courtesy NSIDC; Fetterer et al. 2009); (d) sea ice duration anomaly for 2009, and (e) duration trend (1979–2007). For (d) and (e), see Stammerjohn et al. (2008) for a description of techniques (using daily satellite passive-microwave data). Note that the data used in (d) and (e) are from three different sources: i) 1979–2007 (GSFC Bootstrap dataset, V2); ii) 2008 (F13 Bootstrap daily data); and iii) 2009/10 (NASA Near-Real-Time Sea Ice dataset). However, discrepancies introduced by this factor lead to an uncertainty (difference) level that is well below the magnitude of the large changes/anomalies.

the long-term trend) for the remainder of the year, while the NW Weddell Sea and Bellingshausen Sea switched to positive/near-neutral anomalies. A progressive eastward advection/propagation is also noted in positive anomalies from the W Ross Sea to the Amundsen Sea. This propagation may be consistent with sea ice drift data (under investigation) and, for the Ross-Amundsen Seas, consistent with Assmann et al. (2005).

Consistent with the monthly sea ice extent anomalies (Fig. 6.7a), the ice-edge advance anomalies (not shown) further highlight the late-autumn advance in the Bellingshausen, Western Weddell, and outer central Weddell Sea regions, as well as in East Antarctica between 100°E and 140°E. In contrast, early sea ice advance anomalies are found in most of the Ross Sea and the inner pack ice zone of the Weddell Sea. In further contrast, the ice edge retreat anomalies (also not shown) generally tell a different regional sea ice anomaly story. For example, they show late retreat almost everywhere but in the eastern Ross Sea, the outer pack ice of the Weddell Sea, and the inshore region of the southern Bellingshausen Sea. Thus, as a result, the ice season duration anomaly (Fig. 6.7d) shows a longer ice season in most areas except in East Antarctica (between 100°E and 140°E), the outer western Weddell Sea, and the inshore region in the Bellingshausen Sea.

As highlighted by the sea ice extent anomalies (Fig. 6.7a), the most striking seasonal changes include a switch from late sea ice advance and low sea ice concentration anomalies (blue, Fig. 6.7b) to late sea ice retreat and high sea ice concentration anomalies (red, Fig. 6.7c) in most of the Bellingshausen Sea. This stands in contrast to the switch from early sea ice advance to early sea ice retreat in the western Amundsen/eastern Ross Sea (~140°W–160°W). This seasonal flip in the sign of regional ice anomalies in the high-latitude South Pacific is, however, consistent with moderate La Niña/+SAM conditions prevailing during late 2008/early 2009 versus moderate El Niño/-SAM conditions prevailing late in 2009 (e.g., Stammerjohn et al. 2008; Fogt and Bromwich 2006). Nonetheless, the 2009

positive ice-season duration anomalies for most of the BAS region are in contrast to the strong long-term negative trend in that region, whereas the negative duration anomalies in the outer western Weddell Sea and in East Antarctica (100°E–140°E) are in contrast to the weak but positive trend in those regions (Fig. 6.7e). These negative duration anomalies are however consistent with the eastward "propagation" of ice extent anomalies in the regions in 2009, as described earlier (see Fig. 6.7a). In these regions, i.e., the outer Bellingshausen and western Weddell Seas and East Antarctica, the 2009 anomalies are >2 standard deviations above/below the long-term mean.

g. Ozone depletion—P. A. Newman, E. R. Nash, C. S. Long, M. C. Pitts, B. Johnson, and M. L. Santee

The 2009 Antarctic ozone hole was comparable in size to previous ozone holes. The area of the hole was approximately 22.9 million km^2, about the same size as 2007 and smaller than the 2006 record of 27.7 million km^2. While 2009 was smaller than many recent sizable ozone holes, it is still much larger than values observed prior to 1990. The large area of the ozone hole is consistent with severe depletion caused by the continued high levels of chlorine and bromine in the Antarctic stratosphere. At present, we estimate that ozone depleting substances (ODSs) have only decreased by about 4.3% from the peak levels in the 2000–02 period.

Figure 6.8a displays the average area of the Antarctic ozone hole from 1979 to 2009. The average is calculated by 1) summing the area of the daily values from the Total Ozone Mapping Spectrometer (TOMS) and Aura Ozone Monitoring Instrument (OMI) observations where total ozone values are less than 220 Dobson Units and then 2) averaging the daily estimates from 21–30 September. Using daily SBUV total ozone from the NOAA polar orbiter satellites, the 2009 Antarctic ozone hole was estimated to be the 10th largest on record.

The total ozone values over Antarctica steadily decreased from July to early October 2009. Aura OMI observations showed ozone values of about 236 Dobson Units in July and a low value of 94 Dobson Units on 26 September 2009. Balloon-borne ozonesonde observations from NOAA/ESRL at the South Pole also showed similar behavior. On 25 September, total ozone estimated from the sonde was 98 Dobson Units. The ozonesonde profiles in Fig. 6.8b show that the large losses occurred in the lower stratosphere by late September, with a near complete loss of ozone in the 15–20 km layer on Sep. 29.

The temperature variability of the Antarctic stratosphere modulates the severity of the ozone hole from year to year. Colder-than-average Antarctic temperatures result in larger and deeper ozone holes, while

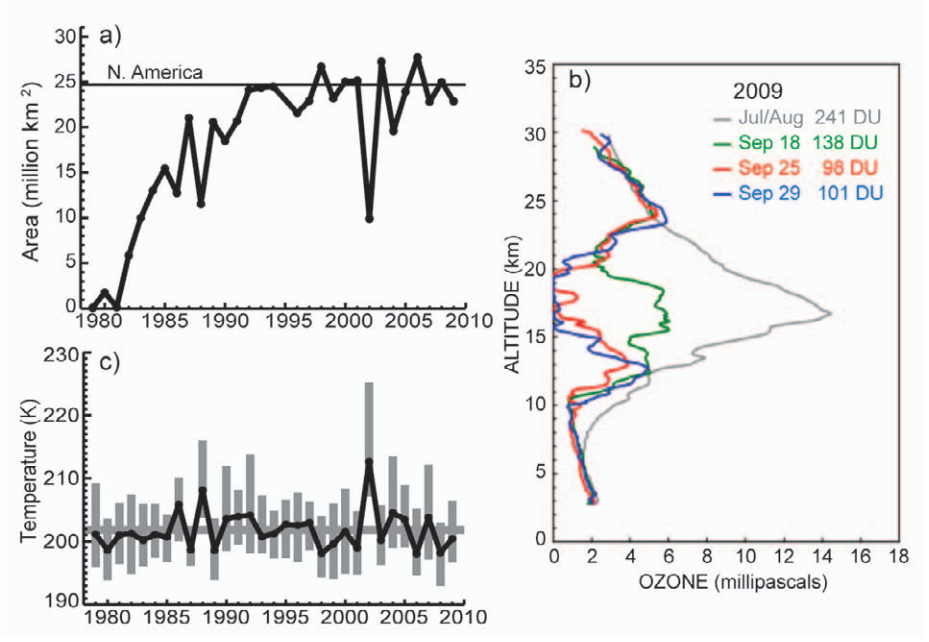

Fig. 6.8. (a) Ozone hole area versus year from 1979 to 2009. The area is determined by first calculating the area enclosed by the 220 Dobson Unit value over the SH for each day from 21 to 30 September, and then averaging these 10 days. The area of the North American continent is indicated by the horizontal bar (24.71 million km^2). (b) Four selected profiles of altitude vs ozone partial pressure (millipascals) measured by ozonesondes at South Pole Station. These 2009 profiles show the pre-ozone hole average in July and August (241 Dobson Units), a mid-September profile, and the minimum values of 98 and 101 DU measured at the end of September. (c) Temperature versus year at 50 hPa from 60°S to 75°S during September. The vertical bars represent the range of values from the individual days of September. The September average over the 1979 to 2009 period is indicated by the horizontal line.

warmer temperatures lead to weaker ozone holes. Fig. 6.8c shows the temperature average (NCEP/DOE reanalysis 2) for September at 50 hPa averaged from 60°S–75°S (edge of the polar vortex). The 2009 September period was near the 31-year average. The cold temperatures in the Antarctic vortex enable the formation of polar stratosphere clouds (PSCs), and these PSCs lead to the activation of reactive chlorine that rapidly destroys ozone as the sun rises over Antarctica.

A fundamental process behind the formation of the ozone hole is the conversion of chlorine molecules from the nonreactive forms (HCl and $ClONO_2$) into ozone reactive forms on the surfaces of PSCs. This reactive chlorine then leads to rapid ozone destruction. The Calipso satellite provides an extremely high-resolution estimate of PSC structure over Antarctica using lidar technology. Calipso observations show that, in terms of season-integrated totals, the 2009 season PSC volume was much less than the record 2006 season and was virtually zero by late September (update from Pitts et al. 2009). The Microwave Limb Sounder (MLS) on the NASA Aura satellite provides information on the chlorine monoxide (ClO) levels inside the Antarctic vortex. In 2009, the chlorine activation was quite high (consistent with high levels of inorganic chlorine from man-made chlorine containing compounds such as chlorofluorocarbons), but less intense, extensive, and persistent than in the last few years.

The Antarctic stratosphere is warmed by the return of sunlight at the end of the polar winter and by large-scale weather systems (planetary-scale waves) that form in the troposphere and move upward into the stratosphere. During the 2009 Antarctic winter and spring, these planetary-scale wave systems were near average for the August–September period. Because the wave levels were near average in 2009, the September Antarctic stratospheric temperatures were also near average as can be seen in Fig. 6.8c.

The 2009 ozone hole was relatively short-lived, with low ozone values disappearing by the end of November. Strong wave forcing in early October and in November caused a dynamically driven warming of the polar stratosphere. By late November into December 2009, lower stratospheric temperatures had risen above average (i.e., Fig. 6.2b) with an accompanying increase of ozone. The ozone hole had virtually disappeared by late November.